CrossMark

Methylene blue removal from aqueous solution by magnetic clinoptilolite/chitosan/EDTA nanocomposite

Fatemeh Aeenjan[1] · **Vahid Javanbakht**[1]

Abstract In this study, clinoptilolite as a natural zeolite which was magnetized using precipitation of maghemite nanoparticles was coated by chitosan and then modified by thylenediamine tetra-acetic acid to add functional groups and its performance in the removal of toxic methylene blue from aqueous solution was investigated. Synthesized magnetic nanocomposite was characterized by VSM, XRD, SEM, and FTIR analyses. The saturation magnetization of the final nanocomposite was obtained as 22.2 emu/g. In addition, the factors affecting adsorption process and its optimization were investigated using response surface methodology and central composite design. Data obtained by different isotherm, adsorption kinetic and thermodynamic models were also studied. The results showed good agreement of these data with the Freundlich isotherm model ($R^2 = 0.99$), and it was found that adsorption follows the second-order kinetics model ($R^2 = 1$). Negative values of ΔG and positive values of ΔH obtained from this adsorption thermodynamic study revealed that the methylene blue adsorption process is exothermic and spontaneous. The optimum conditions to ensure maximum adsorption efficiency were determined, and included pH = 5.54, adsorbent amount of 0.03 g, temperature of 31.18 °C, and initial solution concentration of 16.21 mg/l which resulted in a removal efficiency of 99.44%. The results indicated that this nanocomposite can be used as a proper adsorbent for adsorbing methylene blue and other dye contaminants.

Keywords Methylene blue · Maghemite · Clinoptilolite · Nanocomposite · Adsorption

✉ Vahid Javanbakht
  v.javanbakht@ce.iut.ac.ir

[1] ACECR Institute of Higher Education (Isfahan Branch), Isfahan 84175-443, Iran

Introduction

Dyes are one of the most dangerous chemical compounds found in industrial effluents which are considerably important for reasons including reduction of light penetration followed by disruption of photosynthesis in water resources [1–7]. Environmental pollution is currently considered as a worldwide problem [8–12]. Esthetically, these compounds have negative effects on drinking water quality and its other uses [13, 14], and at the same time cause allergies, dermatitis, skin irritations [15], and cancer [16], as well as genetic mutations in humans [17–21]. Improper treatment and unsystematic disposal of dye wastewater generated by the textile, dyeing, printing and other related industries have led to many environmental problems around the world [22–26]. Removing dye from wastewaters is usually accomplished by physical, physical–chemical, biological or chemical methods [27–31]. Since dye compounds can easily be transferred to a solid phase, adsorption is the most efficient way to remove synthetic dyes from industrial wastewaters [29, 32]. On the other hand, the adsorbent can be restored and used again in the adsorption process or can be stored in dry conditions without direct contact with the environment [33]. In addition, it has been demonstrated that the adsorption process is a reliable treatment approach because of its minimum investment cost, ease of design and operation and lack of susceptibility to toxic compounds [11]. However, given the high prices of some adsorbents, using expensive adsorbents can itself be a limiting factor. Activated carbon [34, 35], porous carbon [36], clay [37, 38], biopolymers such as chitosan [39–41], and byproducts of agricultural activities [42, 43] are adsorbents which have been used for wastewater treatment [44]. Chitosan has a molecular structure similar to cellulose and is composed of a substance called chitin which is found in the shells of oysters and other crustaceans. After cellulose, chitin is the second most abundant biopolymer in nature which has been considered as an appropriate adsorbent for positive dyes. Zeolite is a member of hydrated aluminosilicates of the alkali and alkaline earth metals family and has a tetragonal structure [45]. Considering zeolite's molecular structure, using natural zeolites as adsorbents in many industries has been increasing rapidly and there is ample evidence of practical and industrial applications of this substance, particularly in countries with a long history in mining. Three major properties of zeolites, namely ion-exchange, adsorption and catalytic activity, which are due to their structural features, have been widely used in different branches of industry, especially in environmental processes [45, 46]. Each zeolite is characterized by dimensions of its pores and channels which results in selective adsorption, i.e. adsorption of certain molecules or ions in the presence of other species. Ethylenediamine tetra-acetic acid (EDTA) is a hexadentate chelating agent containing four carboxylic acids and two amino acid groups which surrounds cationic ions and thereby prevents hyper-interaction of particles and inhibits oxidation of cationic ions and the formation of impurity phases. Nowadays, chelating agents are used for long-term synthesis. Since agents are ligands which create stable complexes, this kind of stabilizer has been used in long-term consolidation or commercialization [47].

In this study, natural zeolite clinoptilolite was magnetized by maghemite (γ-Fe_2O_3) magnetic nanoparticles which consist of iron II and III chloride salts as well as NaOH as precipitator. Next, the optimal amount of nanocomposite was coated with chitosan, modified by EDTA and, subsequently, its efficiency in removing methylene blue from aqueous solution was investigated. To evaluate the optimization of factors affecting the adsorption process (pH, temperature, adsorbent amount and concentration of adsorbates), response surface methodology and central composite design was used. Based on the obtained data, different isotherm and kinetic models and thermodynamic studies were also investigated, as discussed later.

Materials and methods

Chemicals

Iron (II) chloride tetrahydrate ($FeCl_2 \cdot 4H_2O$) with 99% purity, Iron (III) chloride hexahydrate ($FeCl_3 \cdot 6H_2O$) with 99% purity, and sodium hydroxide (NaOH) with a purity of 98% were obtained from Merck. Hydrochloric acid (HCl) 37% solution was purchased from SAM CHUNG (South Korea), and powdered clinoptilolite was collected from the central Alborz mountains located in Semnan province in Iran. Average particle size and density of this zeolite were 1 micron and 1.62 g/cm^3, respectively and had the chemical formula of KNa_2Ca_2 (Al_7Si_{29})$O_{72} \cdot 24H_2O$. Chitosan ($C_8H_{13}NO_5$) with 99.9% purity was purchased from Sigma-Aldrich (USA), acetic acid (CH_3COOH) with a purity of 99.7% and sodium chloride (NaCl) with 99.5% purity were obtained from SAM CHUNG. EDTA with 99% purity and methylene blue ($C_{16}H_{18}N_3$) were obtained from Merck.

Preparation of nanocomposite

Before synthesizing the nanocomposite, zeolite was treated to increase maghemite adsorption. 5 g zeolite was put in 5 M HCl solution for 24 h. The processed product was then rinsed with distilled water thrice to reach neutral pH until the acid is thoroughly washed. Then it was dried in an oven at room temperature.

Magnetic maghemite nanoparticles were precipitated on the clinoptilolite by a single-step method [22]. To prepare the nanoparticles, 0.97 g of treated zeolite was poured into 20 ml of distilled water at ambient temperature and was put on the stirrer for 10 min until homogenized. Next, 1.3 g of $FeCl_3 \cdot 6H_2O$ and 0.8 g of $FeCl_2 \cdot 4H_2O$ were homogenized in 20 ml of water for 10 min at room temperature so that the iron salts were dissolved completely. Then, the salts solution and zeolite were mixed together. Next, a basic solution containing 1.6 g of NaOH in 40 ml of water was added dropwise to the prepared suspension for 90 min under inert conditions. Upon completion of the NaOH injection, the dark precipitate was separated from the solution by a strong magnet. The solution was then rinsed once with ethanol and thrice with distilled water and was dried in an oven at 80 °C for 8 h. The nanocomposite of maghemite/clinoptilolite was synthesized with the

weight ratio of 1:1. For the nanocomposite coating, chitosan was used with a weight ratio of 5:1 for the nanocomposite/chitosan. A certain amount of nanocomposite was distributed in 25 ml of water and stirred for 10 min at ambient temperature. Then, 0.1 g of chitosan was dissolved in a 1% acetic acid solution and injected dropwise into the previous suspension for 30 min; 0.5 h later after completion of the covering, it was washed thrice with distilled water to prepare the maghemite/clinoptilolite/chitosan nanocomposite. The product was removed using a magnet and dried in an oven at 70 °C. Finally, to increase the adsorption capacity and modify the surface, the EDTA solution, which includes four carboxylic acid and two amino groups, was added to the nanocomposite. To this end, the nanocomposite was distributed in 25 ml of water and was placed on the stirrer for 10 min. Since EDTA is soluble in basic media, sodium hydroxide was used to dissolve it. Then, the EDTA solution was added dropwise to the nanocomposite (maghemite/clinoptilolite/chitosan) during a 4-h period with a 30-min break until the last drops of EDTA were placed on the nanocomposite. Following injection, the product was magnetically separated, washed twice with NaCl solution and once with distilled water and dried in an oven at 70 °C for 8 h. Finally, the nanocomposite adsorbent (maghemite/clinoptilolite/chitosan/EDTA) was obtained.

Analysis methods

Nanocomposite crystals and phase structures were specified using an X'PertPro X-ray diffractometer (XRD) and irradiation of CuKα ($\lambda = 0.154$ nm) in the range of 10°–90° (2θ). In the XRD method, under specific circumstances, nanometer particle sizes can be determined by the Scherrer equation. In order to evaluate athe dsorbent surface characteristics, a Fourier transform infrared spectrometer (FTIR) JASCO-4200 in the range of 400–4000 cm^{-1} was employed. The composite adsorbent magnetic property was measured through vibrating sample magnetometer (VSM; MPMS-5 SQUID) analyses. Morphological characteristics (shape, size, and arrangement of particles on the object surface) and surface properties of the synthesized sample were assessed using scanning electron microscope (SEM; Zeiss EVO50). The concentration of methylene blue in solution was determined by a RAYLEIGH-UV-2601 spectrophotometer with a maximum wavelength of 664 nm.

Adsorption process

Methylene blue ($C_{10}H_{16}N_2O_8$) was used to prepare the solution for the adsorption assays. First, a stock of 1000 mg/l of methylene blue solution was prepared using distilled water. Then, various dilutions of this solution (2, 5, 10, 15, 20 mg/l) were prepared and 0.1 M NaOH and HCl solutions were used for pH solution adjustment. Overall, a certain amount of magnetic nanocomposite (0.01–0.05 g) was dispersed in 25 ml of methylene blue solution. The nanocomposite and methylene blue mixture were agitated in a shaker at 200 rpm. After the adsorption process, the adsorbent was removed from the solution with the help of a magnet and its adsorption level was measured using a UV spectrophotometer. The adsorbent's

adsorption capacity and dye removal efficiency can be calculated using the following equation [26, 48]:

$$q_e = \frac{(C_0 - C_e) \times V}{M} \tag{1}$$

$$E = \frac{C_0 - C_e}{C_0} \times 100 \tag{2}$$

where q_e is the amounts of dye adsorbed per 1 g of adsorbent, V is the solution volume (l), M is the adsorbent mass (g) and C_e and C_0 are the equilibrium and initial concentrations (mg/l), respectively, and E represents the removal efficiency of methylene blue.

Adsorption kinetic study

Kinetic studies were carried out with the investigation of the concentration decay profile. For this purpose, 0.01 g of synthesized adsorbent was added to 10 ml of 20 mL methylene blue solution. The pH was kept constant on 7 and the mixtures were then put on a shaker for 10, 20, 30, 40, 50, 60, 70, 90, 120, 180, and 240 min at 200 rpm. As time passed, the adsorbent was removed from the solution using a magnet. The qt–t curve was plotted and the data were described using different kinetic models.

Adsorption isotherm study

To determine the adsorption isotherm as well as to study the thermodynamics, the adsorption process was conducted at 25, 40, 55 °C. In the adsorption isotherm experiments, 0.02 g of the nanocomposite was added to 20 ml of methylene blue solution with 10, 20, 30, 40, and 50 mg/l concentrations. The mixtures were then put on a shaker at 200 rpm for 120 min to reach equilibrium. Next, the adsorbent was separated from the solution by a magnet and, finally, with the plot of the q_e–C_e curves, different isotherm models were used for data description.

Results and discussion

Maghemite/clinoptilolite/chitosan/EDTA nanocomposite characterization

SEM analysis was used to evaluate the surfaces and appearance of the samples. Figure 1a shows the surface morphology of clinoptilolite. SEM images of the nanocomposite are represented in (b), (c) and (d). From the (b), (c) and (d) sections, it is evident that maghemite magnetic nanoparticles are present on the clinoptilolite surface and that the chitosan coating has prevented the accumulation and agglomeration of the particles. The samples' XRD patterns were used for phase determination and were compared with recognized standards. Figure 2 displays the XRD results for maghemite nanoparticles and clinoptilolite, and the
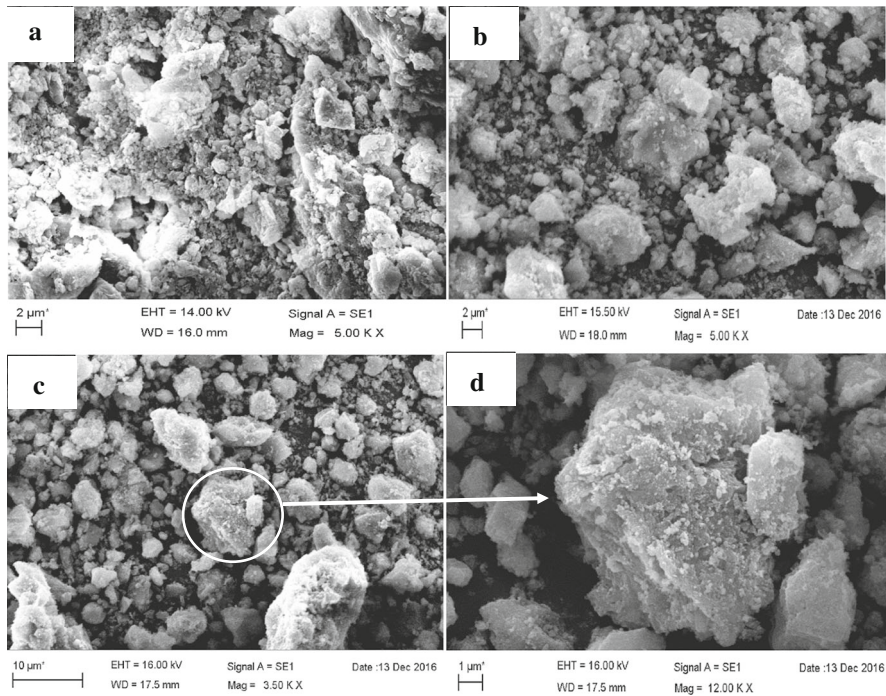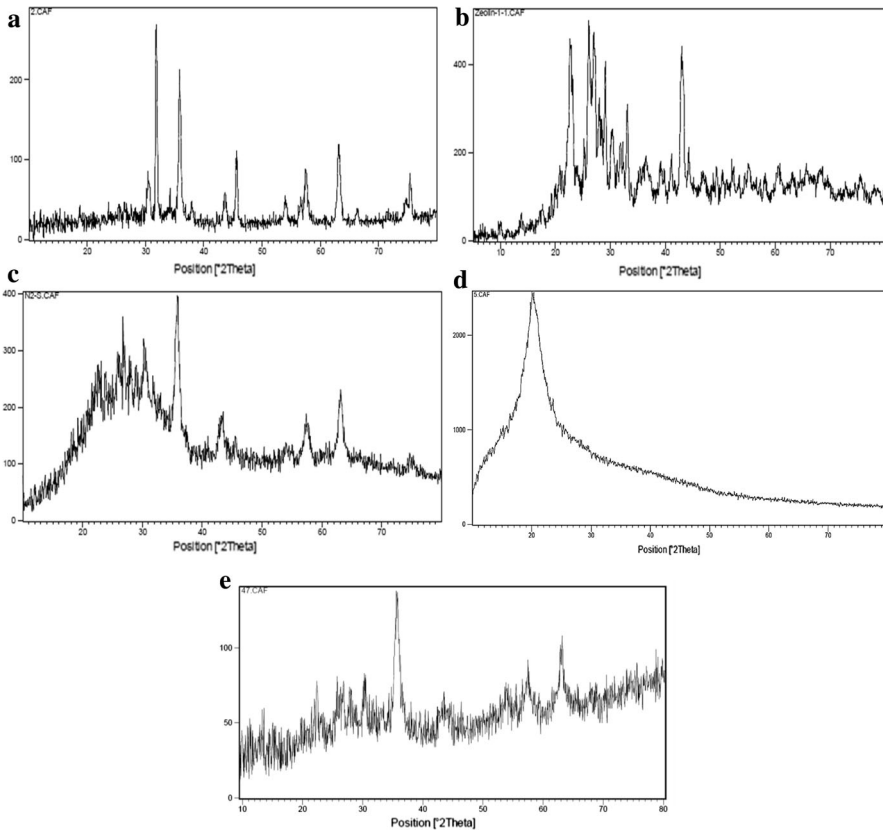
Fig. 1 SEM image of **a** clinoptilolite, **b–d** maghemite/clinoptilolite/chitosan/EDTA nanocomposite

maghemite/clinoptilolite/chitosan and maghemite/clinoptilolite/chitosan/EDTA nanocomposites. Obvious peaks of maghemite at $2\theta = 63.14°$, $57.52°$, $54.01°$, $43.60°$, $35.59°$, $30.51°$, marked by their indices [(2 2 0) (3 1 1), (4 0 0), (4 2 2), (5 1 1) and (4 4 0)] and clinoptilolite peaks at $2\theta = 22.71°$, $26.11°$, and $42.99°$ can be observed in Figs. 4 and 5. In addition, at $2\theta = 20.2°$ a chitosan peak can be observed. The peaks of clinoptilolite (Reference code: 39-1383) and maghemite (Reference code: 39-1346) in the nanocomposite show that the maghemite and clinoptilolite found in this nanocomposite have retained their original structures. The EDTA coating has also not caused any changes, including chemical ones, to the nanocomposite structure and it is completely obvious that the EDTA peaks have increased. The results of using the Scherrer formula for average particle size calculations based onthe XRD data curve revealed that the nanoparticles' size is about 14 nm. In the Scherrer formula:

$$D = \frac{K\lambda}{\beta cos\theta} \tag{3}$$

D is the average particle size (nm), K is the crystal shape factor (0.9), λ is the wavelength of the X-ray tube (if CuKα radiation is used, it equals to 0.154 nm), β is the peak's full width at half maximum height and θ is the diffraction angle.

The results obtained from VSM for the synthesized samples are shown in Fig. 3. As can be seen, all the curves are *S*-shaped which implies that the nanocomposite is
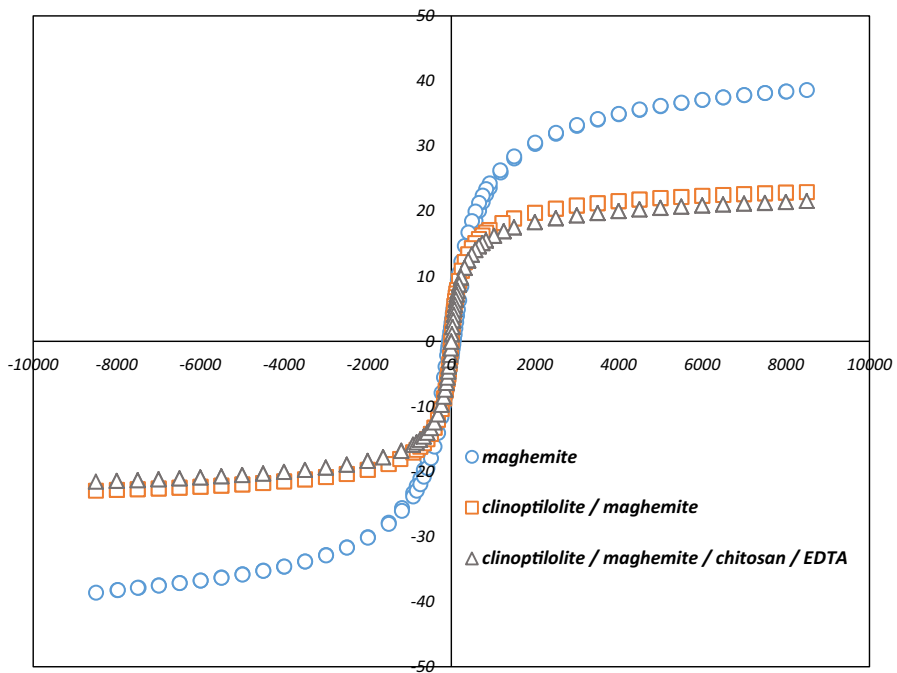
Fig. 2 XRD results of **a** maghemite, **b** clinoptilolite, **c** maghemite/clinoptilolite nanocomposite, **d** chitosan, **e** maghemite/clinoptilolite/chitosan/EDTA nanocomposite

superparamagnetic. Saturation magnetization represents the ease of sample removal from aqueous suspension after using zeolite in desired processes, which is considered one of the advantages of this synthesized nanocomposite. On the other hand, increasing the zeolite content in the nanocomposite decreases the saturated magnetic field because magnetism varies with maghemite content in the nanocomposite. This suggests that adding non-magnetic elements to maghemite leads to a reduction of nanocomposite magnetic property. According to the VSM curve, it can be concluded that saturation magnetization of maghemite magnetic nanoparticles (38.2 emu g^{-1}) is more than that of the clinoptilolite/maghemite (24.3 emu g^{-1}) and maghemite/clinoptilolite/chitosan/EDTA nanocomposites (22.2 emu g^{-1}).

IR analysis was used to determine the type of synthesized materials and their functional groups as well as to demonstrate the success of the nanocomposite coating. Figure 4a shows that the adsorption visible at 797–1641 cm^{-1} is the result of the stretching and bending modes of Si–O or Al–O bonds within the clinoptilolite structure [49]. The peak appearing at 3436 cm^{-1} is related to the stretching vibration caused by hydrogen bonds created by hydroxide groups (OH) [50]. From

Fig. 3 VSM results of maghemite (circles), maghemite/clinoptilolite nanocomposite (squares), and maghemite/clinoptilolite/chitosan/EDTA nanocomposite (triangles)

Fig. 4b, it can be concluded that the bond around 3396 cm^{-1} within the maghemite spectrum could be associated with the stretching mode of H$_2$O molecules or hydroxyl groups on the surface of the maghemite nanoparticles. It is also obvious that the peak around 1617 cm^{-1} is linked to the vibrating bonds of H$_2$O. Metal–oxygen bonds observed at 579 and 424 cm^{-1} are related to the tetrahedral and octagonal stretching modes of the metal, respectively. Figure 4c shows the infrared spectrum of the clinoptilolite/maghemite nanocomposite. Strong adsorption peaks at 450 and 570 cm^{-1} which belong to the Fe– O bond show that maghemite is formed. In general, wavelengths below 700 cm^{-1} are associated with the Fe–O bond [51]. Our findings reveal that the spectrum of the zeolite/maghemite nanocomposite is no different from that of zeolite. As is evident from Fig. 4, H–C bond vibrations have given peaks at 2423 and 2923 cm^{-1} within the chitosan spectrum. Peaks observed in 1417, 1383, and 1085 cm^{-1} can be assigned to the C–N stretching vibration. Figure 4d demonstrates that peaks centered at 3443, 2800, 1698, 1411, and 1147 cm^{-1} in the EDTA spectrum are apparently related to the stretching bonds of N–H, C–H, –C=C–, C–O and C–N, respectively [52]. The infrared spectrum of the maghemite/clinoptilolite/chitosan/EDTA nanocomposite is shown in Fig. 4f. In addition to the adsorption characteristics of the bonds of the chitosan functional groups, there is a peak at 570 cm^{-1} which is caused by the Fe–O bond. Adsorption peaks in the 1000–1400 cm^{-1} region, which include peaks observed at 1061 and 1383 cm^{-1}, are attributed to the stretching vibration of N–C [53]. Since the
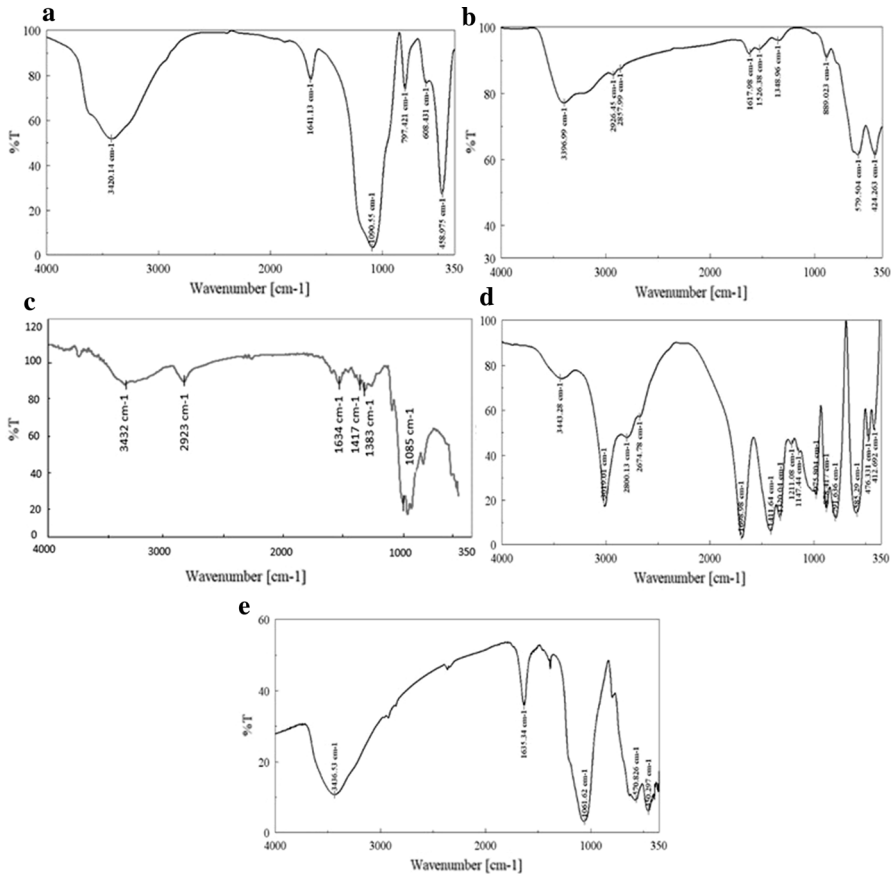
Fig. 4 FTIR results of **a** clinoptilolite, **b** maghemite, **c** maghemite/clinoptilolite nanocomposite, **d** EDTA, **e** maghemite/clinoptilolite/chitosan/EDTA nanocomposite

adsorption peaks found at 1650–1800 cm^{-1} region are related to the C=O stretching vibration, the peaks existing at 1635 cm^{-1} in the spectra of chitosan and the nanocomposite can be assigned to the C=O bond [54]. The bending vibration of the H–N bond also gives a peak at 3460 cm^{-1}.

Adsorption studies

Adsorption kinetics study

One of the most important factors in designing a sorption system is to predict the adsorption rate and the time it takes to reach equilibrium. A kinetics study gives us valuable insights into this issue [55]. Thus, pseudo-first- and -second-order kinetic models, intra-particle diffusion and Elovich models were used for the adsorption kinetics study discussed below. The pseudo-first-order kinetic model describes the rate of adsorption based on adsorption capacity. This equation is used to express the

adsorption rate of an adsorbate in an aqueous solution. Pseudo-first-order rate equations are based on adsorbent capacity and are applied when the adsorption is accompanied by diffusion through a boundary layer. The linear form of this equation is as follows [56]:

$$\log(q_e - q_t) = \log q_e - k_1 \times t \tag{4}$$

where q_e and q_t are the amounts of solute adsorbed in the solid phase at equilibrium and at time t (mg g^{-1}), respectively, and k_1 is the rate constant of pseudo-first-order adsorption (min^{-1}).

If $\ln(q_e - q_t)$ is drawn against time for laboratory conditions, a straight line will be obtained from which the rate constant, k_1, and the correlation coefficient, R^2, can be determined.

Pseudo-second-order rate equations are used for the analysis of chemical kinetics, the adsorption of metal ions in aqueous solutions, etc. The pseudo-second-order equation indicates that chemical sorption is the dominant and controlling mechanism in the adsorption process, and that the rate-limiting step in the solid phase. The linear form of the equation is expressed as [57, 58]:

$$\frac{t}{q_t} = \frac{1}{k_2 q_e^2} + \frac{t}{q_e} \tag{5}$$

With $k_2 q_e^2 = h$, we have:

$$h = k_2 q_e^2 \tag{6}$$

where q_e and q_t are the amounts of solute adsorbed in the solid phase at equilibrium and at time t (mg g^{-1}), respectively, and k_2 is the rate constant of pseudo-second-order adsorption (min^{-1}). By plotting t/q_e against t, k_2 and R^2 can be calculated. Pseudo-first- and -second-order models consist of the penetration in external film, intraparticle diffusion, and interaction between metal ions and the absorbent's functional groups. Intraparticle diffusion is a transitional process which describes the motion of particles from solution to the solid phase.

$$q_t = k_i t^{0.5} + C \tag{7}$$

where k_i and C denote the intraparticle motion constant and diffusion rate constant of the boundary layer, respectively. The Ellovich model is used to interpret chemical kinetics and is defined as follows:

$$q_t = \frac{1}{\beta} \ln(\alpha \beta) + \frac{1}{\beta} \ln t \tag{8}$$

where α and β are the initial adsorption/desorption rate constant of surface coating and the activation energy of chemical adsorbent, respectively [49].

According to Fig. 5a, in the beginning, the rate of adsorption is very high so that, in the first 10 min, more than 80% of methylene blue was separated from the solution. The results show that, as time passes, the percentage of removal and adsorption capacity increase while the adsorption intensity decreases. This increase
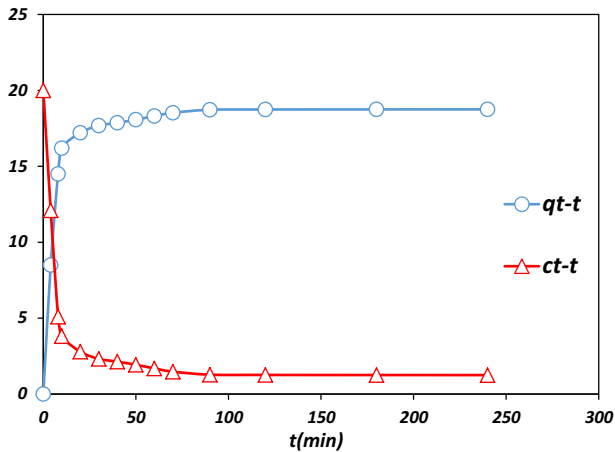
Fig. 5 Kinetic data of methylene blue adsorption on the nanocomposite

in adsorption capacity continues until the system reaches equilibrium. After that, adsorption of methylene blue becomes stable as the adsorbent becomes saturated.

Based on Fig. 5a, the adsorbent reaches equilibrium in the first 120 min and shows a nearly constant trend in the next 120 min. This means that the adsorbent surface is covered by a layer of methylene blue and the repulsive force between methylene blue molecules and mass molecules has led to adsorption rate reduction. The constants for kinetic models (Fig. 6a–d) are listed in Table 1. The values obtained (R^2) from the kinetic models that are presented in Table 1 suggest that the adsorption process complies more with the pseudo-second-order kinetic model. Thus, it can be concluded that chemical adsorption is rate-controlling and adsorption of methylene blue is a result of interactions between functional groups on the adsorbent surface and is not caused by a diffusion mechanism [49]. Intraparticle diffusion is a transitional process which describes the motion of solute particles from solution to the solid phase. Figure 6d shows that the methylene blue adsorption process is more than just one diffusion step. Moreover, $K_{i,1} > K_{i,2} > K_{i,3}$ implies three different steps of methylene blue adsorption, at the outer surface, the inner surface, and equilibrium, respectively.

Adsorption isotherm study

Four isotherm models, of Langmuir, Freundlich, Temkin, and Dubinin–Radushke-vich, were used to evaluate the adsorption isotherms. The Freundlich isotherm model which can be used to characterize heterogeneous adsorption systems is:

$$\ln q_e = \ln k_f + \frac{1}{n} \ln C_e \tag{9}$$

where k_f and n denote Freundlich constants for the maximum adsorption capacity and heterogeneous factor, respectively. The Langmuir model has been successfully applied to a large number of single-layer adsorption processes. It assumes that
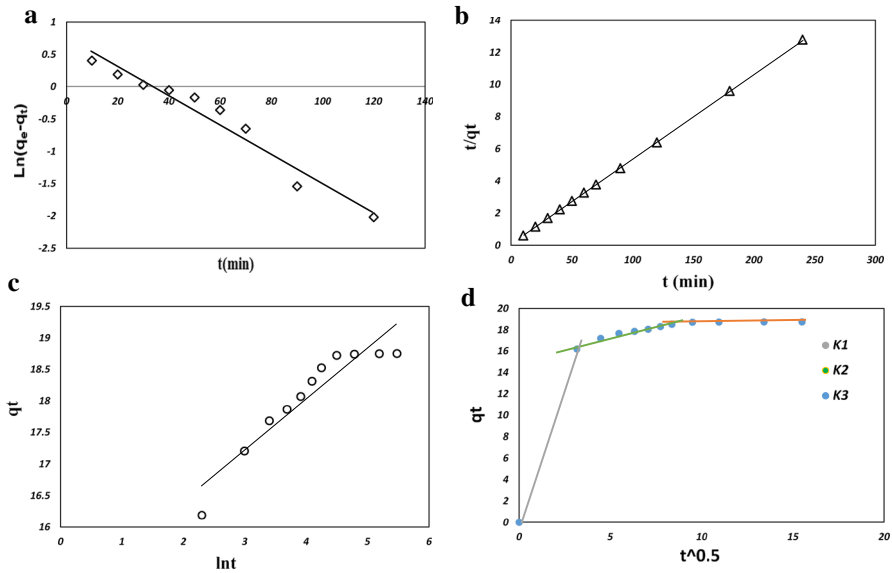
Fig. 6 Plots of pseudo-first-order, pseudo-second-order, Elovich and intraparticle diffusion kinetic models of methylene blue adsorption on the nanocomposite

adsorption occurs at particular homogeneous sites of the adsorbent. This model can be expressed as follows:

$$\frac{C_e}{q_e} = \frac{1}{k_1 q_{max}} + \frac{1}{q_{max}} \tag{10}$$

where q_{max} and k_1 represent the maximum adsorption capacity (mg/g) and Langmuir adsorption constants, respectively. The Dubinin–Radushkevich model is used for the identification of chemical and physical adsorption and is defined as:

$$\ln q_e = \ln q_m - B\varepsilon^2 \tag{11}$$

In which q_{max} is the maximum capacity to adsorb the solute, β is a constant rated to the adsorption average energy and ε is given by the following equation:

$$\varepsilon = RT \ln\left(1 + \frac{1}{C_e}\right) \tag{12}$$

where R is the universal gas constant (8.314 J/mol k) and T is the temperature. Free energy of transferring 1 mol of solution from infinity to the adsorbent surface, i.e. average energy E, can be calculated by the following equation:

Table 1 Kinetic parameters of different kinetic models for methylene blue adsorption on the nanocomposite

Pesudo-first-order			Pesudo-second-order				Elovich			Intraparticle diffusion						
K_1	q_e	R^2	K_2	Q_e	h	R^2	A	β	R^2	Ki_1	R_1^2	Ki_2	R^2	Ki_3	R_3^2
0.022	2.16	0.95	0.02796	10.007	18.93	1	2.19	1.2	0.88	5.12	1	0.3	0.98	0.002	0.99

$$E = \frac{1}{\sqrt{2\beta}} \qquad (13)$$

The Temkin isotherm assumes that the adsorption temperature decreases linearly rather than logarithmically with increasing the adsorbent surface coating. This model is given by:

$$q_e = \frac{RT}{b_T} \ln(AT) + \frac{RT}{b_T} \ln C_e \qquad (14)$$

where b_T is a constant related to the adsorption heat and A is a constant related to the adsorption potential. Drawing the models' curves shows that the adsorption isotherm complies with the Langmuir model [49]. Methylene blue adsorption with the same adsorbent amount at different temperatures and concentrations is plotted in Fig. 7. The results obtained from the adsorption parameters (Fig. 8) in Table 2 indicate that the adsorption behavior of methylene blue on the nanocomposite is more consistent with the Freundlich model. The Freundlich isotherm empirical equation is based on non-uniform, heterogeneous multilayer adsorption [59].

Adsorption thermodynamics study

Another measure that is especially important in describing the adsorption process is the determination of thermodynamic parameters. The thermodynamic parameters such as enthalpy changes (kJ/mol), entropy changes (J/mol K), and Gibbs free energy changes (kJ/mol) are determined using the following equation:

$$\ln K_d = -\frac{\Delta H}{RT} + \frac{\Delta S}{R} \qquad (15)$$

$$\Delta G = -RT \ln K_d \qquad (16)$$
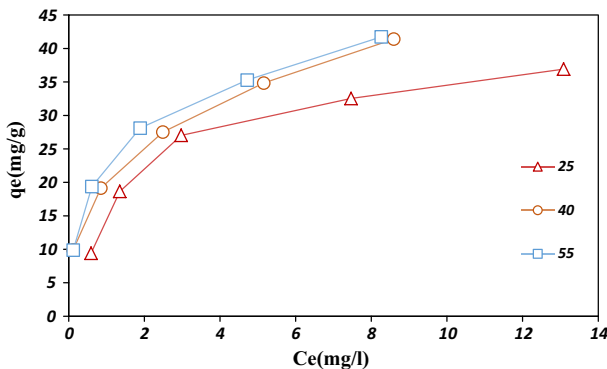
Fig. 7 Isotherm data of methylene blue adsorption on the nanocomposite at different temperatures (25, 40 and 55 °C)
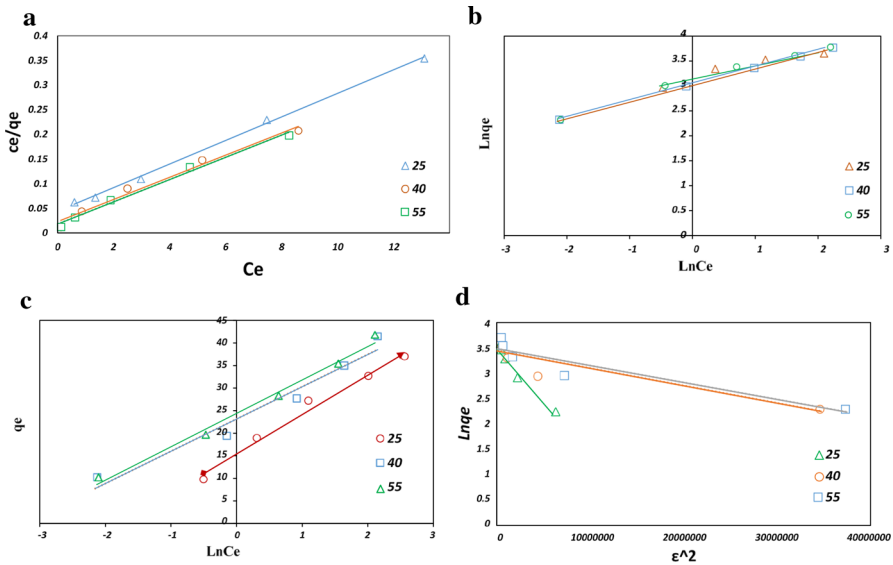
Fig. 8 Isotherm models of methylene blue adsorption on nthe anocomposite at different temperatured (25, 40 and 55 °C): **a** Langmuir, **b** Freundlich, **c** Temkin, and **d** Dubinin–Radushkevich

Table 2 Isotherm parameters of different isotherm models for methylene blue adsorption on the nanocomposite

| T (°C)	Freundlich			Langmuir			Temkin			Dubinin–Radashkevich		
	R^2	n	K_f	q_m	K_1	R^2	b_T	A	R^2	B	q_m	R^2
25	3	20.23	1	41.84	0.54	0.99	8.73	5.82	0.98	2E−07	32.34	0.95
40	3.77	23.05	0.93	44.44	38.46	0.98	7.15	3.55	0.95	3E−08	32.63	0.87
55	2.97	21.42	0.99	44.24	11.24	0.989	7.40	26.9	0.987	3E−08	31.18	0.82

In which R is the universal gas constant, T is the temperature (K) and K_d (= q_e/C_e) is the equilibrium constant at different temperatures [60]. As Fig. 9 shows, plotting $\ln K_d$ against $1/T$ gives a straight line from which ΔH and ΔS can be calculated from its slope and intercept, respectively. Values of Gibbs free energy, enthalpy, and entropy changes are presented in Table 3. According to Table 3, negative values of ΔG indicate that adsorption bythe maghemite/clinoptilolite/chitosan/EDTA nanocomposite is spontaneous. Moreover, positive values of ΔS represent an increase of random encounters between the adsorbent/solution phases during adsorption of methylene blue. ΔH positive values also reveal that the adsorption process is endothermic and that the adsorption temperature increases as the efficiency increases [61].
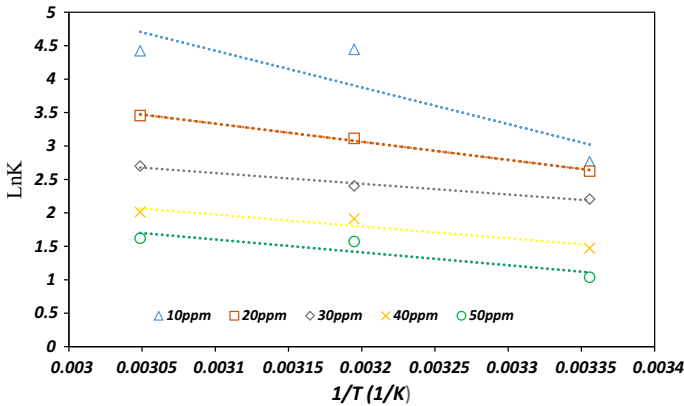
Fig. 9 Thermodynamic plots of methylene blue adsorption on the nanocomposite

Table 3 Thermodynamic parameters of methylene blue adsorption on the nanocomposite

C (mg/l)	T (K)	ΔH (KJ/mol)	ΔS (J/mol)	ΔG (KJ/mol)
10	298	45.598	178.15	− 10.95
	313			− 8.99
	328			− 7.36
20	298	22.530	97.57	− 8.56
	313			− 7.02
	328			− 5.48
30	298	13.329	62.90	− 6.69
	313			− 5.23
	328			− 4.41
40	298	14.760	62.18	− 4.98
	313			− 4.97
	328			− 4.01
50	298	15.977	62.84	− 4.01
	313			− 4.09
	328			− 2.82

Design of experiments

Experimental design is a set of tests which purposefully make changes in the input variables of a process in order to explore and observe possible changes in the output response. As there is a need to use methods to reduce the number of required tests and accelerate the logical conclusion, deploying experimental design is necessary. An accurate design not only reduces costs but also paves the way to achieve reliable results. The interesting point is that in this way of analyzing experiments, the results become easier and more accurate which is as good as the experimental procedures. In order to achieve the optimum condition of methylene blue adsorption, 30

Table 4 The levels of CCD

Variable	Levels		
pH	4	5	6
Temperature (°C)	30	40	50
Methylene blue concentration (mg/l)	15	20	25
Adsorbent amount (g)	0.01	0.025	0.05

experiments with different conditions were designed by Design Expert software using the CCD method. The experiments were carried out within a 120-min period and the results are presented in Table 5. The effects of features such as the adsorbent amount, the concentration of methylene blue, the temperature and the solution pH were investigated. The levels of the parameters are shown in Table 4. The expected response in these tests was considered to be the efficiency of methylene blue removal.

Following kinetic, isotherm and thermodynamic adsorption tests, and after assessing the appropriate operating range of the process, the experimental design was used to find a suitable adsorption model in terms of various operational parameters. The first step in the validation of the results was the analysis of variance (ANOVA) which was performed with the aim of evaluating the statistical significance and finding the best model to assess the most important factors affecting the response and to identify interactions. This technique uses some tests to examine the influence of parameters and their interactions in the process. The importance of each parameter was evaluated using F values and these are presented in Table 6, which also shows the results of ANOVA on which the type of model can be determined. The higher F values and lower P values represent the greater importance of the relevant parameter. In general, for each model, if the P value is less than 0.05, the model is appropriate and statistically significant [62]. It also becomes clear which parameters have the greatest influence on the design. Here, the main first-order effects of pH, initial concentration, and adsorbent amount, the second-order effects of the adsorbent amount, the initial concentration of methylene blue and the interaction effect between pH and adsorbent amount are important terms of the model. The results suggest that the regression is statistically significant at F value = 26.78 and P value < 0.0001.

The accuracy and conformity of the model were evaluated by the determination coefficient denoted by R^2. Here, R^2 equals 0.9615 which is acceptable. R^2 specifies how well the model fits the experimental data; the closer it is to 1 the more robust the model and the better the response and prediction. The adjusted coefficient of determination, R^2adj, is a measure of how well the regression line represents the data. R^2 and R^2adj values are very close to each other. This closeness between these values indicates that any insignificant independent variables of the model have been excluded. A relatively low coefficient of variation (5.79) shows good accuracy and reliability of tests. The Adeq Precision parameter measures the accuracy of the signal-to-noise ratio for which a value of 4 is considered to be acceptable. The achieved value of 17.075 represents an accurate ratio.

Table 5 The data of design of experiments

Run	pH	Temperature (°C)	Initial concentration (mg/l)	Amount of adsorbent (g)	Removal efficiency (%)
1	4	30	15	0.02	42.90
2	6	30	15	0.02	95.89
3	4	50	15	0.02	63.63
4	6	50	15	0.02	96.87
5	4	30	25	0.02	48.36
6	6	30	25	0.02	92.25
7	4	50	25	0.02	49.22
8	6	50	25	0.02	92.62
9	4	30	15	0.04	96.36
10	6	30	15	0.04	98.15
11	4	50	15	0.04	98.02
12	6	50	15	0.04	99.63
13	4	30	25	0.04	91.39
14	6	30	25	0.04	97.92
15	4	50	25	0.04	96.96
16	6	50	25	0.04	98.18
17	3	40	20	0.03	40.34
18	7	40	20	0.03	98.81
19	5	20	20	0.03	96.09
20	5	60	20	0.03	93.67
21	5	40	10	0.03	98.64
22	5	40	30	0.03	93.84
23	5	40	20	0.01	72.85
24	5	40	20	0.05	97.88
25	5	40	20	0.03	96.66
26	5	40	20	0.03	98.14
27	5	40	20	0.03	96.77
28	5	40	20	0.03	97.14
29	5	40	20	0.03	97.09
30	5	40	20	0.03	97.75

The equation model related to the removal of methylene blue is reported based on the influencing independent variables. The final correlation for the parameters is expressed by the following equation:

$$\begin{aligned} \text{Removal} = &-425.2 + 120.0 \times \text{pH} + 8161.2 \times \text{Adsorbent dosage} - 1014.7 \\ &\times \text{Initial solution pH} \times \text{Adsorbent dosage} - 32{,}428.1 \\ &\times \text{Adsorbent dosage2} \end{aligned} \quad (17)$$

Table 6 ANOVA of methylene blue adsorption on the nanocomposite

	Sum of the squares	df	Mean square	F value	P value, Prob > F
Model	9673.62	14	690.97	26.78	< 0.0001
A Initial solution pH	3790.86	1	3790.86	146.90	< 0.0001
B Temperature (°C)	30.49	1	30.49	1.18	0.2942
C initial solution concentration (mg/l)	48.65	1	48.65	1.89	0.1899
D Adsorbent (g)	2499.61	1	2499.61	96.86	< 0.0001
AB	41.38	1	41.38	1.60	0.2247
AC	1.84	1	1.84	0.071	0.7929
AD	1647.35	1	1647.35	63.84	< 0.0001
BC	19.74	1	19.74	0.76	0.3956
BD	12.16	1	12.16	0.47	0.5029
CD	5.16	1	5.16	0.20	0.6610
A^2	1418.07	1	1418.07	54.95	< 0.0001
B^2	20.48	1	20.48	0.79	0.3871
C^2	7.57	1	7.57	0.29	0.5961
D^2	288.43	1	288.43	11.18	0.0044
Residual	387.09	15	25.81		
Lack-of-fit	385.45	10	38.55	117.49	< 0.0001
Pure error	1.64	5	0.33		
Corr. total	10,060.71	29			

Analysis of statistical plots

The statistical plots related to methylene blue adsorption on the maghemite/clinoptilolite/chitosan/EDTA nanocomposite are shown in Fig. 10. Figure 10a shows the actual values versus the predicted response values. The values which are not predictable by the model can be determined using this figure, in which points around the regression line must have a homogenous distribution. Figure 10b shows the residual adsorption of methylene blue according to which the residual values are well distributed around the regression line. This means that the majority of the data exist around the middle line, which indicates that the data are not dispersed. In Fig. 10c, the residual values are plotted against the predicted response values related to the adsorption of methylene blue within which it is assumed that the points are distributed randomly. Figure 10d shows the residual values studentized in terms of the observation sequence of methylene blue adsorption. In this figure, the residual values should be randomly distributed around the center line and their distribution should not follow any specific pattern.
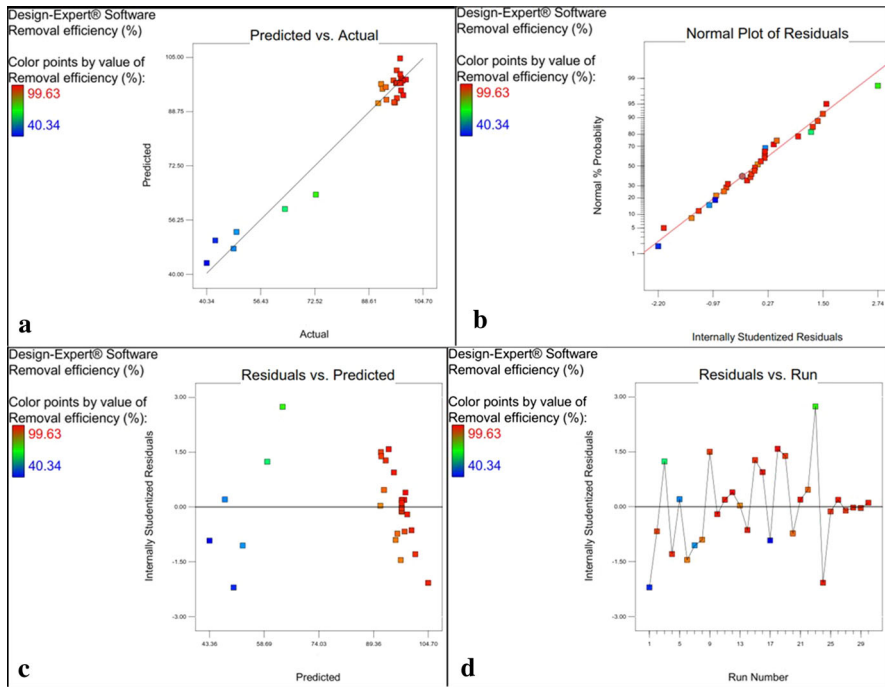
Fig. 10 **a** The actual and predicted methylene blue removal capacity, **b** the studentized and normal percentage probability plots of ethylene blue removal capacity, **c** the predicted removal and the studentized residual plot, and **d** the run number and the studentized residual plot

Study of parameters effects on the adsorption

The pH is an important chemical factor that affects the adsorption process through influencing the adsorbent surface charge [63]. Choosing suitable pH results in optimal adsorption efficiency and increases the adsorption rate. In acidic pH, adsorbents attract hydrogen ions and become positively charged. When the solution pH increases, the number of accessible positively charged sites decreases and the number of negatively charged sites increases. Interactions between cationic dye molecules and adsorbents increases as the adsorbent becomes more negatively charged. So, the adsorption capacity of the adsorbent increases with increasing pH value [64]. Reduction of methylene blue adsorption with increasing adsorbent amount can be explained by two reasons. First, despite increasing adsorption-active sites with increasing the adsorbent amount, the adsorbed ions to adsorbent mass unit decreases because the number of adsorbed ions is constant. Second, as the adsorbent amount increases and the adsorbent particles become accumulated and agglomerated, the adsorption-active sites may become inaccessible to the methylene blue ions [65]. By increasing the initial concentration of the methylene blue solution, the

concentration difference which is the adsorption driving force [65] increases and subsequently the methylene blue adsorption increases. In fact, methylene blue ions can bind to the adsorption sites on the adsorbent surface and increase the adsorbability of the adsorbent. At higher concentrations of adsorbed ions, adsorption sites are occupied and adsorption of methylene blue is reduced and becomes slower [66]. Studies have shown that the adsorption increase is caused by a temperature increase which leads to: (1) the rapid and better diffusion of adsorbed dye ions in the outer layer and the internal pores of the adsorbent particles, (2) increasing the mobility of the dye ions, (3) increasing the number of dye ions that can obtain enough energy to interact with active sites of the adsorbent surface, (4) inflation of the internal structure of the adsorbent which enables larger dye particles to penetrate more into the absorbent, and (5) solubility of the dye ions which significantly affects the adsorption process. It is noteworthy that increasing the adsorption capacity caused by temperature growth indicates that the adsorption process is in nature an endothermic process. Given the stated reasons and experimental results, the more the temperature rises the more methylene blue is removed [67, 68]. As can be seen in Fig. 11a, with the adsorbent amount of 0.02 g and initial concentration of methylene blue equal to 15 mg/l, the removal increases with increasing pH at a given temperature. Figure 11b shows a 3-D graph of the effects of initial concentration and pH on methylene blue adsorption. At higher concentrations, the adsorbent sites are occupied by adsorbed ions and methylene blue removal is decreased. Also, asthe pH increases from 4 to 6, H_3O+ ions decline and –OH ions increase, the positive ligands bind to the –OH ions and subsequently electrostatic desorption of positive dye ions decreases. Moreover, with decreasing H_3O+ ions, methylene blue adsorbs by negative ligands on the adsorbent surface whereby removal increases. Figure 11c represents the effects of adsorbent amount and pH on methylene blue removal. It is obvious that removal increases as the adsorbent amount increases from 0.02 to 0.04 g and the pH increases from 4 to 6. Thus, the highest removal is achieved by the simultaneous increase in pH and adsorbent amount. A 3-D graph of the effects of temperature and initial concentration on methylene blue removal is shown in Fig. 11d, where it can be seen that, as the temperature and initial concentration of methylene blue increase, removal increases. The reason behind this is explained in the previous sections. Figure 11e displays a 3-D graph of the effects of temperature and adsorbent amount on methylene blue removal. The reason for this is described in the previous sections. The 3-D graph of effects of adsorbent amount and initial concentration parameters on methylene blue removal is demonstrated in Fig. 11f. As one can see, methylene blue removal increases with adsorbent amount while adsorption increases with initial concentration.

## Optimization of the adsorption process

After analyzing the results, the optimum conditions to achieve maximum adsorption efficiency were determined. To this end, taking into consideration the optimal points of major variables within the levels specified for responses, maximum values were defined. Maximum removal efficiency and variables correlation and optimal
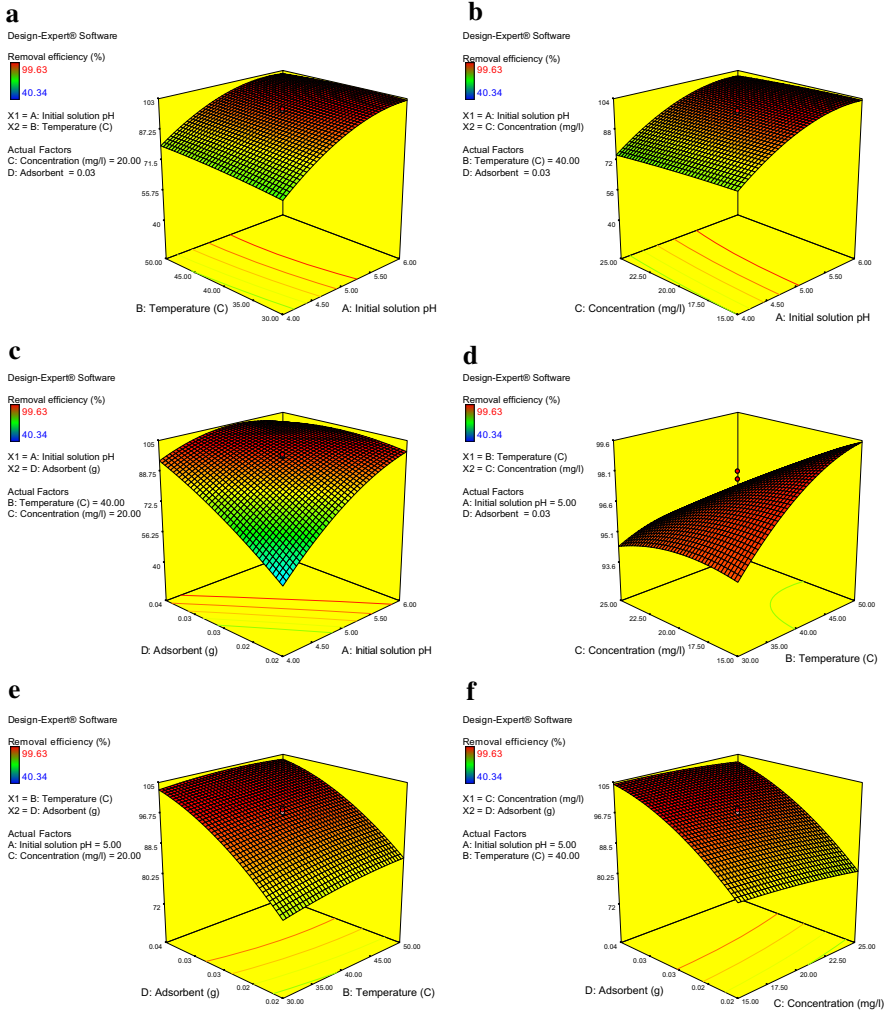
Fig. 11 3-D response surface plots for the effect of: **a** pH and temperature (°C), **b** pH and initial concentration (mg/L), **c** pH and adsorbent dosage (g/L), **d** temperature (°C) and initial concentration (mg/L), **e** temperature (°C) and adsorbent dosage (g/L), and **f** initial concentration (mg/L) and adsorbent dosage (g/L) on the methylene blue removal

conditions were determined using numerical optimization [49]. Figure 12 shows the schematic model of optimal conditions, variable values, and responses. The optimum conditions included pH = 5.54, adsorbent amount of 0.03 g, temperature of 31.18 °C, and solution initial concentration of 16.21 mg/l, which resulted in a highly efficient removal of 99.44%.
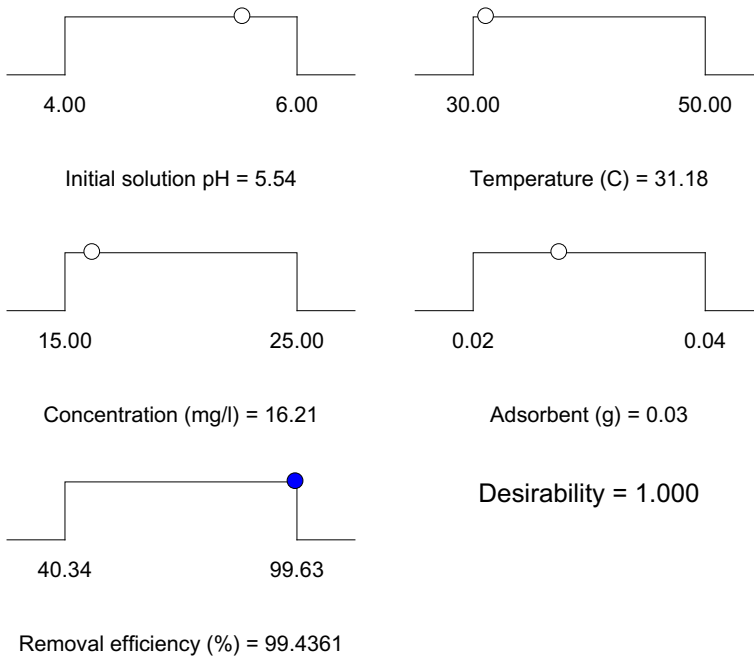
Fig. 12 The optimization of the response and the variables

Conclusions

In this study, zeolite clinoptilolite was magnetized by maghemite magnetic nanoparticles which consist of iron II and III chloride salts as well as NaOH as precipitator, and was coated by chitosan and modified EDTA, and its effectiveness in the removal of methylene blue from aqueous solution was investigated. The synthesized magnetic nanocomposite was characterized by VSM, XRD, SEM, and FTIR analyses. The saturation magnetization of the final nanocomposite was obtained as 22.2 emu/g. The nanocomposite was readily separated from solution using a quick and simple magnetic separation process. In addition, based on the obtained data, different isotherm and kinetic models and thermodynamic investigations were studied and it was found that the Data corresponded better with the Freundlich adsorption model and that adsorption follows the pseudo-second-order kinetic model. Negative values of ΔG and positive values of ΔH obtained from the adsorption thermodynamic study revealed that the methylene blue adsorption process is spontaneous. Moreover, response surface methodology and central composite design were used to examine the factors affecting the adsorption process and its optimization. The optimum conditions to ensure maximum adsorption efficiency were determined and included pH = 5.54, dsorbent amount of 0.03 g, temperature of 31.18 °C, and solution initial concentration of 16.21 mg/l which resulted in a removal of 99.44%. The results indicated that this nanocomposite can

be used as a proper adsorbent for adsorbing methylene blue and other dye contaminants.

References

1. B. Royer, N.F. Cardoso, E.C. Lima, J.C. Vaghetti, N.M. Simon, T. Calvete, R.C. Veses, J. Hazard. Mater. **164**(2), 1213 (2009)
2. E.C. Lima, B. Royer, J.C. Vaghetti, N.M. Simon, B.M. da Cunha, F.A. Pavan, E.V. Benvenutti, R. Cataluña-Veses, C. Airoldi, J. Hazard. Mater. **155**(3), 536 (2008)
3. M. Ahmaruzzaman, V.K. Gupta, Ind. Eng. Chem. Res. **50**(24), 13589 (2011)
4. T.A. Saleh, V.K. Gupta, J. Colloid Interface Sci. **371**(1), 101 (2012)
5. D. Zhu, J. Zhang, J. Song, H. Wang, Z. Yu, Y. Shen, A. Xie, Appl. Surf. Sci. **284**, 855 (2013)
6. R. Saravanan, M.M. Khan, V.K. Gupta, E. Mosquera, F. Gracia, V. Narayanan, A. Stephen, J. Colloid Interface Sci. **452**, 126 (2015)
7. R. Saravanan, F. Gracia, M.M. Khan, V. Poornima, V.K. Gupta, V. Narayanan, A. Stephen, J. Mol. Liq. **209**, 374 (2015)
8. J. Paul, K. Rawat, K. Sarma, S. Sabharwal, Appl. Radiat. Isot. **69**(7), 982 (2011)
9. R. Saravanan, S. Karthikeyan, V. Gupta, G. Sekaran, V. Narayanan, A. Stephen, Mater. Sci. Eng. C **33**(1), 91 (2013)
10. V. Gupta, A. Nayak, Chem. Eng. J. **180**, 81 (2012)
11. V.K. Gupta, R. Kumar, A. Nayak, T.A. Saleh, M. Barakat, Adv. Colloid Interface Sci. **193**, 24 (2013)
12. R. Saravanan, E. Sacari, F. Gracia, M.M. Khan, E. Mosquera, V.K. Gupta, J. Mol. Liq. **221**, 1029 (2016)
13. B. Royer, N.F. Cardoso, E.C. Lima, T.R. Macedo, C. Airoldi, J. Hazard. Mater. **181**(1), 366 (2010)
14. V.K. Gupta, T.A. Saleh, Environ. Sci. Pollut. Res. **20**(5), 2828 (2013)
15. D.S. Brookstein, Dermatol. Clin. **27**(3), 309 (2009)
16. R.O.A. de Lima, A.P. Bazo, D.M.F. Salvadori, C.M. Rech, D. de Palma Oliveira, G. de Aragão Umbuzeiro, Mutat. Res./Genet. Toxicol. Environ. Mutagen. **626**(1), 53 (2007)
17. P.A. Carneiro, G.A. Umbuzeiro, D.P. Oliveira, M.V.B. Zanoni, J. Hazard. Mater. **174**(1), 694 (2010)
18. A. Mittal, J. Mittal, A. Malviya, V. Gupta, J. Colloid Interface Sci. **340**(1), 16 (2009)
19. R. Saravanan, V. Gupta, T. Prakash, V. Narayanan, A. Stephen, J. Mol. Liq. **178**, 88 (2013)
20. R. Saravanan, E. Thirumal, V. Gupta, V. Narayanan, A. Stephen, J. Mol. Liq. **177**, 394 (2013)
21. R. Saravanan, N. Karthikeyan, V. Gupta, E. Thirumal, P. Thangadurai, V. Narayanan, A. Stephen, Mater. Sci. Eng. C **33**(4), 2235 (2013)
22. I. Koyuncu, Desalination **143**(3), 243 (2002)
23. H.-L. Liu, Y.-R. Chiou, J. Chin. Inst. Chem. Eng. **37**(3), 289 (2006)
24. V.K. Gupta, R. Jain, A. Nayak, S. Agarwal, M. Shrivastava, Mater. Sci. Eng. C **31**(5), 1062 (2011)
25. D. Balarak, J. Jaafari, G. Hassani, Y. Mahdavi, I. Tyagi, S. Agarwal, V.K. Gupta, Colloids Interface Sci. Commun. **7**, 16 (2015)
26. A. Mittal, J. Mittal, A. Malviya, V. Gupta, J. Colloid Interface Sci. **344**(2), 497 (2010)
27. K. Vijayaraghavan, Y.-S. Yun, Dyes Pigm. **76**(3), 726 (2008)
28. C. Namasivayam, D. Kavitha, Dyes Pigments **54**(1), 47 (2002)
29. N. Mohammadi, H. Khani, V.K. Gupta, E. Amereh, S. Agarwal, J. Colloid Interface Sci. **362**(2), 457 (2011)
30. R. Saravanan, V. Gupta, V. Narayanan, A. Stephen, J. Taiwan Inst. Chem. Eng. **45**(4), 1910 (2014)
31. A. Mittal, D. Kaur, A. Malviya, J. Mittal, V. Gupta, J. Colloid Interface Sci. **337**(2), 463 (2009)
32. V.K. Gupta, A. Mittal, D. Jhare, J. Mittal, RSC advances **2**(22), 8381 (2012)
33. J.C. Vaghetti, E.C. Lima, B. Royer, J.L. Brasil, B.M. da Cunha, N.M. Simon, N.F. Cardoso, C.P.Z. Noreña, Biochem. Eng. J. **42**(1), 67 (2008)
34. P.K. Malik, J. Hazard. Mater. **113**(1), 81 (2004)
35. E. Demirbas, M. Kobya, M. Sulak, Bioresour. Technol. **99**(13), 5368 (2008)

36. D.D. Asouhidou, K.S. Triantafyllidis, N.K. Lazaridis, K.A. Matis, S.-S. Kim, T.J. Pinnavaia, Microporous Mesoporous Mater. **117**(1), 257 (2009)
37. S. Lambert, N. Graham, C. Sollars, G. Fowler, Water Sci. Technol. **36**(2–3), 173 (1997)
38. N. Lazaridis, T. Karapantsios, D. Georgantas, Water Res. **37**(12), 3023 (2003)
39. M.-S. Chiou, H.-Y. Li, J. Hazard. Mater. **93**(2), 233 (2002)
40. S. Rosa, M.C. Laranjeira, H.G. Riela, V.T. Fávere, J. Hazard. Mater. **155**(1), 253 (2008)
41. A. Jain, V. Gupta, A. Bhatnagar, Suhas, Sep. Sci. Technol. **38**(2), 463 (2003)
42. X.S. Wang, Y. Zhou, Y. Jiang, C. Sun, J. Hazard. Mater. **157**(2), 374 (2008)
43. F. Çiçek, D. Özer, A. Özer, A. Özer, J. Hazard. Mater. **146**(1), 408 (2007)
44. T.A. Saleh, V.K. Gupta, Sep. Purif. Technol. **89**, 245 (2012)
45. S. Kocaoba, Y. Orhan, T. Akyüz, Desalination **214**(1–3), 1 (2007)
46. R. Roque-Malherbe, Microporous Mesoporous Mater. **41**(1), 227 (2000)
47. Z. Ezzeddine, I. Batonneau-Gener, Y. Pouilloux, H. Hamad, Z. Saad, V. Kazpard, Microporous Mesoporous Mater. **212**, 125 (2015)
48. G.-N. Moroi, E. Avram, L. Bulgariu, Water Air Soil Pollut. **227**(8), 1 (2016)
49. V. Javanbakht, S.M. Ghoreishi, N. Habibi, M. Javanbakht, Powder Technol. **302**, 372 (2016)
50. S. Mopoung, Int. J. Phys. Sci. **3**(10), 234 (2008)
51. E. Darezereshki, Mater. Lett. **64**(13), 1471 (2010)
52. R.G. López, M.G. Pineda, G. Hurtado, R.D.d. León, S. Fernández, H. Saade and D. Bueno. Int. J. Mol. Sci. **14**(10), 19636 (2013)
53. K. Azizi, M. Karimi, F. Nikbakht, A. Heydari, Appl. Catal. A Gen. **482**, 336 (2014)
54. Y. Liu, M. Chen, H. Yongmei, Chem. Eng. J. **218**, 46 (2013)
55. S. Yang, J. Li, D. Shao, J. Hu, X. Wang, J. Hazard. Mater. **166**(1), 109 (2009)
56. D.J. O'Shannessy, D.J. Winzor, Anal. Biochem. **236**(2), 275 (1996)
57. Y.-S. Ho, G. McKay, Process Biochem. **34**(5), 451 (1999)
58. H. Zheng, Y. Wang, Y. Zheng, H. Zhang, S. Liang, M. Long, Chem. Eng. J. **143**(1), 117 (2008)
59. U. Freundlich, J. Phys. Chem. **57**, 385 (1906)
60. H. Hou, R. Zhou, P. Wu, L. Wu, Chem. Eng. J. **211**, 336 (2012)
61. Y.-M. Hao, C. Man, Z.-B. Hu, J. Hazard. Mater. **184**(1), 392 (2010)
62. N. Yahaya, M. Pakir, M. Latiff, I. Abustan, O. Bello, M. Ahmad Int, J. Eng. Technol. **10**, 132 (2010)
63. M.V. Dinu, E.S. Dragan, Chem. Eng. J. **160**(1), 157 (2010)
64. W.W. Ngah, L. Teong, M. Hanafiah, Carbohyd. Polym. **83**(4), 1446 (2011)
65. V. Javanbakht, H. Zilouei, K. Karimi, Int. Biodeterior. Biodegradation **65**(2), 294 (2011)
66. V. Javanbakht, S.M. Ghoreishi, Adsorpt. Sci. Technol. **35**(1–2), 241 (2017)
67. D. Nimkar, S. Chavan, Int. J. Eng. Res. Appl. **4**, 47 (2014)
68. A. Özer, G. Dursun, J. Hazard. Mater. **146**(1), 262 (2007)